15th Australasian Fluid Mechanics Conference
The University of Sydney, Sydney, Australia
13-17 December 2004

The Internal Wave Field Generated by the Body and Wake of a Horizontally Moving Sphere in a Stratified Fluid

James W. Rottman[1], Dave Broutman[2], Geoff Spedding[3] and Patrice Meunier[3]

[1]Science Applications International Corporation
San Diego, CA 92121 USA

[2]Computational Physics, Inc.
Springfield, VA 22151 USA

[3]Department of Aerospace and Mechanical Engineering
University of Southern California, Los Angeles, CA 90089-1191 USA

Abstract

A combination of ray and Fourier methods is used to describe the linear internal wavefield generated by a horizontally moving, vertically oscillating, source in a stratified fluid. Ray theory is used to approximate the wavefield in a Fourier transform domain. The ray solutions are then superimposed by inverse Fourier transform to produce the spatial solution. This is a more practical approach than calculating the ray solution directly in the spatial domain, and it is general enough to treat background flows with depth dependent shear and stratification. The theory is compared with tank experiments for a towed sphere in a uniformly stratified background.

Introduction

Obstacles that move through a stratified fluid generate internal waves, either directly by the displacement of the fluid around the obstacle or indirectly by motions in the obstacle's wake. The wake motions consist of turbulent eddies and the collapse of partially mixed regions toward an equilibrium density level.

To gain insight into these generation processes, we study the case of a source travelling horizontally at constant speed through a vertically stratified fluid. We consider moderate Froude number $Fr = U/(Na)$, where U is the speed of the source, a is its radius, and N is the buoyancy frequency of the fluid.

The theory, described in more detail in [2], is a modification of the methods developed for topographically generated internal waves by [1] and [2]. Ray solutions are computed in a Fourier transform domain and are then superimposed by inverse Fourier transform to produce a spatial solution. This is a more practical approach than calculating the ray solution directly in the spatial domain, mainly because the Fourier superposition automatically accounts for diffraction effects near caustics and other regions where the spatial ray theory fails.

We present the theory in a form that allows the source to oscillate vertically as well as move horizontally. The vertical oscillations will be used to model the unsteady wave generation by turbulence in the wake of the sphere, as suggested by [3]. The theory is developed for a depth-dependent background, but in this study the results presented are limited to a uniform background. This is to compare with our available data from laboratory experiments, which were conducted by towing a sphere through a background at rest with uniform stratification. Wave reflections from the upper and lower boundaries of the tank are important, so the reflected waves are included in the theory.

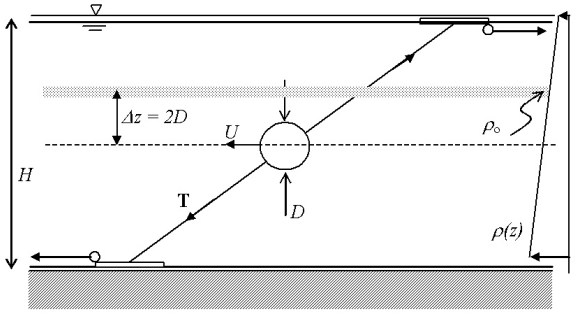

Figure 1: A sphere of diameter D is towed horizontally at speed U through a linear density gradient in water of depth H. Wave motions propagate away from the sphere and through a carpet of neutrally-buoyant polystyrene beads with density ρ_0. In the experiments reported here, the beads are 2 sphere diameters above the midplane of the sphere. Model vibrations are reduced by operating at high tension **T** in the oblique support wires.

Theory

We consider a stratified Boussinesq fluid. Internal waves are generated by a source that moves horizontally at constant speed while oscillating vertically at constant frequency σ. The coordinate system, $\mathbf{r} = (x,y,z)$ with z positive upwards, is fixed to the mean position of the oscillating source. The background flow in this reference frame is $\mathbf{U} = (U(z), V(z), 0)$, and the background buoyancy frequency is $N(z)$.

The internal waves have wavenumber $\mathbf{k} = (k,l,m)$ and intrinsic frequency

$$\hat{\omega} = \sigma - kU - lV. \tag{1}$$

The internal-wave dispersion relation is

$$m = \pm (k^2 + l^2)^{1/2} (N^2/\hat{\omega}^2 - 1)^{1/2}. \tag{2}$$

We derive a solution for the vertical displacement $\tilde{\eta}(k,l,z)$ of the wavefield at a fixed horizontal wavenumber. The spatial solution is then obtained by inverse Fourier transform:

$$\eta(\mathbf{r},t) \quad = \quad e^{-i\sigma t} \iint_{-\infty}^{\infty} \tilde{\eta}(k,l,z)\, e^{i(kx+ly)} dk\, dl\ . \tag{3}$$

The factor $e^{-i\sigma t}$ accounts for all of the time dependence in the present model. This can be considered as the long-time limit

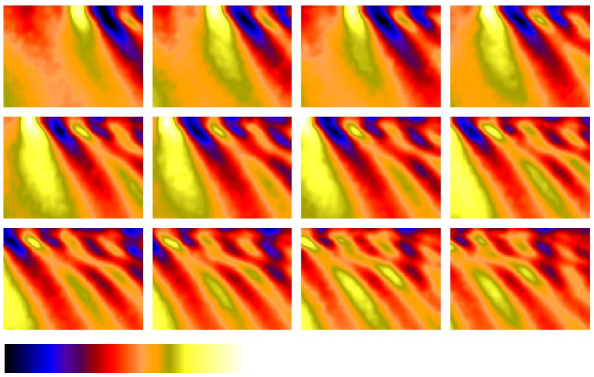

Figure 2: Experimental results for u in the case of $Fr = 2$. Each image is a horizontal cross section of one side of the wake. The 12 images are for equally spaced times over the duration of time $Nt = 29.8$. Time increases from left to right and from top to bottom. The total distance traversed by the sphere in this time is $29.8D$. The minimum and maximum values for u are -0.2cm/s to 0.14cm/s.

of an initial value problem in which the motion is started from rest, and the associated transients have decayed or propagated away.

We use a ray approximation for $\tilde{\eta}(k,l,z)$, of the form

$$\tilde{\eta}(k,l,z) = b(k,l,z)\, e^{i\int_0^z m(k,l,z')dz'}. \tag{4}$$

The amplitude $|b|$ can be derived from the conservation of wave-action A, which here reduces to the constancy of the vertical flux of wave-action $c_{g3}A$, where $c_{g3} = \partial\hat{\omega}/\partial m$ is the vertical group velocity.

The details of the derivation are given in [2]. Here we quote the result:

$$b = \pi i (Q/\hat{\omega})_0 \, [G_0/G]^{1/2}. \tag{5}$$

The zero subscript indicates evaluation at $z = 0$, the mean depth of the source. We also have

$$G = N^2 c_{g3}/\hat{\omega}, \tag{6}$$

For the source function Q, we use the following form, from [3],

$$Q(\mathbf{k},t) = \frac{3}{4} i\pi^{-2} a^3 \left[U_0 k + h\sigma e^{-i\sigma t} m\right] \frac{j_1(Ka)}{Ka}, \tag{7}$$

where $K = |\mathbf{k}|$ and $j_1(z) = (\sin z)/z^2 - (\cos z)/z$ is the spherical Bessel function of order unity. The background flow at the mean position of the source is U_0, which is aligned in the x-direction. In the limit of large Froude number $Fr = U_0/Na$ the source function (7) represents the effects of a horizontally translating, vertically oscillating, solid sphere of radius a. The amplitude of the vertical oscillation of the sphere is h, and its vertical velocity is $h\sigma e^{-i\sigma t}$.

Modifications of the above results to incorporate buoyancy frequency turning points (where $\hat{\omega} = N$) are given in [1] and [2].

To compute the spatial solution for another variable, such as the x-component of the perturbation velocity u, we need only to relate the vertical displacement $\tilde{\eta}$ to $\tilde{u}$ by standard ray relations (e.g. [5]) before taking the inverse Fourier transform (3).

Reflected Waves

So far we have only considered waves that move upward from the source. To compare with our experimental results, we must allow wave reflections from the upper and lower boundaries of the tank. From here on, we will restrict attention to a uniform background, which is the condition of the experiments.

To account for wave reflections, we follow the method of [1], where more details can be found. Consider a fixed height z above the source and a tank of height H. Each time a ray returns to that z after reflecting once from the top of the tank and once from the bottom of the tank, the wave phase mz is advanced by $m2H$. To include the effects of this and subsequent reflections, we must multiply $\hat{\eta}(k,l,z)$ in (4) by the sum

$$S = \sum_{n=0}^{\infty} e^{in2mH} \tag{8}$$

$$= ie^{imH}/2\sin mH. \tag{9}$$

The sum is defined in the sense of generalized functions (see Eq. (1.2.2) of [6]). It diverges for $mH = \pi$, the condition for perfect constructive interference between all of the reflected waves. The divergence can be eliminated by adding a small damping factor in the form of an imaginary wavenumber m_i, as in [1], or by limiting S to a finite number of terms. The number of terms can be chosen to represent a finite number of reflections at the time of interest, as determined by group velocity calculations. We have so far only experimented with the first method. In the results presented below, we have used a value of $m_i H = 0.02$.

The wavefield, including all reflected waves, is modelled by four terms, each with a factor of S. Two terms represent upward and downward moving rays that initially leave the source moving upward. The other two terms represent upward and downward moving rays that initially leave the source moving downward. The term $\hat{\eta}(k,l,z)S$, where $\hat{\eta}(k,l,z)$ is given by (4), corresponds to the first of those four terms.

Experiments

Experiments were conducted in a 2.4×2.4 m tank filled to a height $H = 26$cm with a linearly stratified salt solution. The density gradient was created by the standard two-tank method, and density values were checked at an array of taps in the sidewall. In the experiments reported here, the buoyancy frequency $N = 1.88 \pm 2\%$. The sphere was towed at a height of 11.3cm above the bottom tank. The sphere diameter is $D = 2.52$cm and $Fr = N/Ua$ (where $a = D/2$) was varied by varying the tow speed U. For $Fr = 1$, the tow speed was $U = 2.37$cm/s. The Reynolds number Re varies by the same amount (i.e. for $Fr = 1,2,4$, we have $Re = 600, 1200, 2400$), but we assume the variations in Re to be of minor importance for the wavefield. A horizontal (isopycnal) bead sheet is left at a height $\Delta z = 2D$ above the mid-plane of the sphere, and particle motions are tracked using a custom DPIV technique, detailed in [4] and [7]. The experimental setup is sketched in figure 1.

To improve the spatial and temporal resolution, the image window was centered on one side of the wake only (assuming bilateral symmetry), and exposures were made over fast and slow timescales using a nested pair of short and long exposure times at each timestep. The components of the horizontal velocity field u, v were calculated directly from the particle image displacements and interpolated onto a regular grid by a two-dimensional smoothing spline.

Results

We will consider the cases of $Fr = 1, 2, 4$. The sphere is towed in the x direction, and each plot that we present is a horizontal

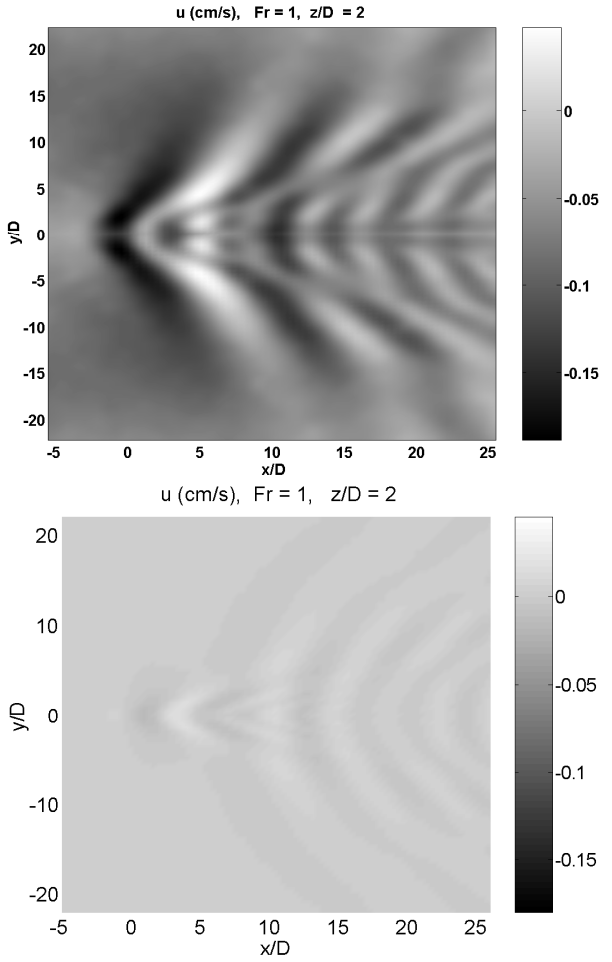

Figure 3: A comparison for $Fr = 1$ of tank experiments (upper panel) and theory (lower panel). The plotted variable is u, the x-component of the velocity of the wavefield, in cm/s.

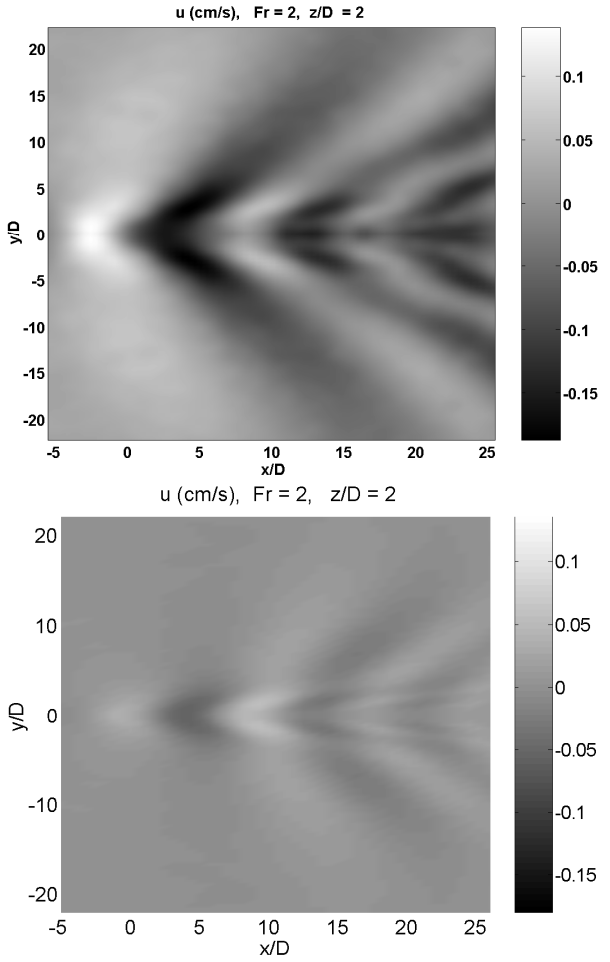

Figure 4: A comparison for $Fr = 2$ of the experimental result (upper panel) and the theory (lower panel). The plots are of u.

cross section at a height $z = 2D$ above the centerplane of the sphere. All plots are of the x component u of the wavefield velocity. In all plots except the final figure 6, we have considered a non-oscillating source, i.e. $\sigma = 0$ in (7).

For the theoretical calculation, the inverse Fourier transform (3) was approximated discretely on a Fourier grid of 1024 x 1024 in k, l. The corresponding grid spacing in the spatial domain is about 0.8cm. A smaller number of Fourier grid points would have sufficed in some cases. In addition to resolving the flow features, the extent of the Fourier grid must be chosen to limit periodic wrap-around errors, which result from the discrete approximation of the inverse Fourier transform.

A sequence of images of u from the tank experiment is shown in figure 2 for the case of $Fr = 2$. Here and in subsequent figures, the image grid size is 74 x 54, with spacing 1.072 cm x 1.056 cm. This gives a 78.3 x 56 cm window (inside a 2.44 x 2.44 m tank). In units of D the window is $31D$ x $22.2D$. The window is fixed in space and the sphere moves through it in time.

As noted above, the images from the experiments were taken on one side of the wake only, assuming a symmetric wake. In the following figures, we have flipped the experimental images symmetrically to give the more familiar picture of the full wavefield. The data points directly behind the obstacle, along the line $y = 0$, are at the edge of the field of measurement, and this shows up as an anomaly in the following figures.

Figure 3 is for the case of $Fr = 1$. The tank measurement is shown in the top panel, and our linearized theory is shown in the lower panel. At this relatively low Froude number the turbulent eddies in the wake are not strong and are thus not important for the generation of internal waves. (We ignore wake generation until figure 6). However, the source function we have used, (7), is most accurate for the representation of a solid sphere only in the limit of high Froude number. Thus some of the discrepancy between the theory and measurements in this example may be due to the source representation. In the future, we plan to try other source representations that depend on the Froude number.

Figure 4 shows the case of $Fr = 2$, again with the experimental results in the upper panel and the theory in the lower panel. The peak theoretical amplitude of the wavefield is lower than the peak amplitude of the experiments, by a factor of about two. This difference in wave amplitudes is maintained in the region closest to the obstacle, so the difference must be due to factors other than turbulent eddy generation in the wake. We have omitted from the theory all eigenfunctions that correspond to evanescent modes. These could be included in the theory, by the usual WKB methods, and might account for some of the difference in the amplitude predictions. Another possibility is the presence of vortical modes, which may be important in the experimental results but are not included in the theory. We plan to check this by comparing the horizontal divergence $u_x + v_y$ of the experimental data and the theory, which would reveal the

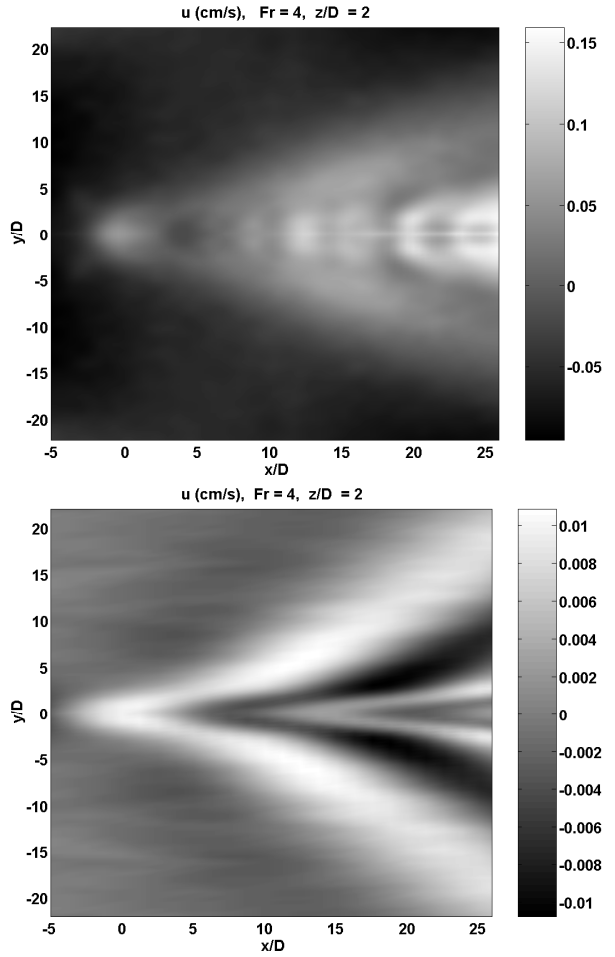

Figure 5: A comparison for $Fr = 4$ of the experimental result (upper panel) and the theory (lower panel). The plots are of u.

non-vortical modes only.

Figure 5 shows the results for $Fr = 4$. Here our linear theory is a poor representation of the experimental results, though it does give a reasonable prediction for the lateral extent of the wavefield. This is the parameter regime in which eddy-generated internal waves from the wake are important. A better agreement between theory and experiment is obtained by including an oscillating source to model the eddy generation. Previously we had ignored the oscillating term in the source function (7). Here we include the oscillating term, with oscillation amplitude $h = 0.4a$ and frequency $\sigma = 2.5N$, following guidelines in [3]. The result is shown in figure 6, which is a better fit to the data, though the theory predicts a wavefield that is more concentrated around the x-axis.

Conclusions

This work is a step toward seeing how far ray theory can go in simulating the internal wavefield generated by an obstacle and its wake. By combining ray and Fourier methods, we have obtained a detailed three-dimensional picture of the wavefield, with far higher resolution than possible in numerical models. The calculation is also fast, taking only a few seconds for each depth on a standard PC. Future needs are a better representation of the source, dependent on the Froude number, and a more detailed study of the effectiveness of modelling wake generated internal waves by an oscillating source.

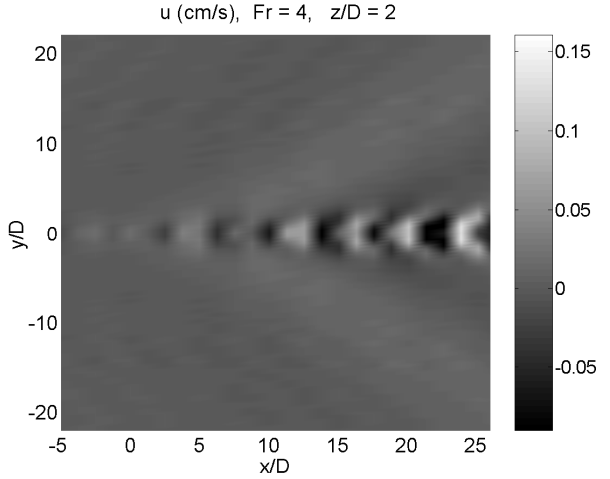

Figure 6: As in Figure 5, lower panel, but with an additional oscillating source term for wave generation by wake eddies.

Acknowledgements

This research is supported by ONR under contract numbers N00014-01-C-0191 and N00014-96-1-0001. Dr. Ronald Joslin is the program manager.

References

[1] Broutman, D., Rottman, J. and Eckermann, S., A simplified fourier method nonhydrostatic mountain waves, *J. Atmos. Sci.*, **60**, 2003, 2686–2696.

[2] Broutman, D. and Rottman, J., A simplified fourier method for computing the internal wavefield generated by an oscillating source in a horizontally moving, depth-dependent background, *Phys. Fluids*, **16**, 2004, 3682–3689.

[3] Dupont, P. and Voisin, B., Internal waves generated by a translating and oscillating sphere, *Dyn. Atmos. Oceans*, **23**, 1996, 289–298.

[4] Fincham, A. and Spedding, G., Low-cost high-resolution dpiv for turbulent flows, *Exps. Fluids*, **23**, 1997, 449–462.

[5] Gill, A., *Atmosphere-Ocean Dynamics*, Academic Press, 1982.

[6] Hardy, G., *Divergent Series*, Clarendon, 1949.

[7] Spedding, G., Browand, F. and Fincham, A., Turbulence, similarity scaling and vortex geometry in the wake of a towed sphere in a stably stratified fluid, *J. Fluid Mech.*, **314**, 1996, 53–103.